Ngwenya, B.T. et al. (2009) *Macroscopic and spectroscopic analysis of lanthanide adsorption to bacterial cells.* Geochimica et Cosmochimica Acta, 73 (11). pp. 3134-3147. ISSN 0016-7037

http://eprints.gla.ac.uk/5689/

Deposited on: 15 June 2009

Macroscopic and Spectroscopic Analysis of Lanthanide Adsorption to Bacterial Cells.

Bryne T. Ngwenya[1], J. Fred W. Mosselmans[2], Marisa Magennis[1+] , Kirk D. Atkinson[2#],
Janette Tourney[1§], Valerie Olive[3] and Robert M. Ellam[3].*

[1]Environmental and Microbial Geochemistry Laboratory,
School of Geosciences,
University of Edinburgh,
West Mains Road,
Edinburgh EH9 3JW,
United Kingdom.

[2]Diamond Light Source Ltd,
Diamond House,
Chilton,
Didcot,
Oxfordshire OX11 0DE,
United Kingdom

[3]Scottish Universities Environmental Research Centre,
Rankine Avenue,
East Kilbride,
G75 0QF,
United Kingdom

* Corresponding author

[+]Now at: The School of Physics, University of Edinburgh, James Clerk Maxwell Building, Edinburgh EH9, United Kingdom..

[#]Now at: Defence College of Electro-Mechanical Engineering, HMS Sultan GOSPORT, Hampshire, PO12 3BY, United Kingdom.

[§]Now at: School of Engineering, Durham University, South Road, Durham DH1 3LE, United Kingdom..

Abstract

This study was designed to combine surface complexation modelling of macroscopic adsorption data with X-ray Absorption Spectroscopic (XAS) measurements to identify lanthanide sorption sites on the bacterial surface. The adsorption of selected representatives for light (La and Nd), middle (Sm and Gd) and heavy (Er and Yb) lanthanides was measured as a function of pH, and biomass samples exposed to 4 mg/L lanthanide at pH 3.5 and 6 were analysed using XAS. Surface complexation modelling was consistent with the light lanthanides adsorbing to phosphate sites, whereas the adsorption of middle and heavy lanthanides could be modelled equally well by carboxyl and phosphate sites. The existence of such mixed mode coordination was confirmed by Extended X-ray Absorption Fine Structure (EXAFS) analysis, which was also consistent with adsorption to phosphate sites at low pH, with secondary involvement of carboxyl sites at high adsorption density (high pH). Thus, the two approaches yield broadly consistent information with regard to surface site identity and lanthanide coordination environment. Furthermore, spectroscopic analysis suggests that coordination to phosphate sites is monodentate at the metal/biomass ratios used. Based on the best fitting pKa site, we infer that the phosphate sites are located on N-acetylglucosamine phosphate, the most likely polymer on gram-negative cells with potential phosphate sites that deprotonate around neutral pH.

1 Introduction

Despite a decade of experimental studies involving adsorption of metals to bacterial surfaces, the mechanistic basis of the adsorption reactions remains an open question. Early experimental studies relied almost exclusively on surface complexation modelling to postulate reaction stoichiometry and the identity of surface sites to which the metals were

78   adsorbed (Fein et al., 1997; Daughney et al., 1998; Fowle & Fein, 1999; Haas et al., 2001;

79   Ngwenya et al., 2003; Yee et al., 2004). Central to this postulate was the assumption that

80   surface functional groups must deprotonate to generate a negative surface site before

81   positively charged metal ions could adsorb (Fein et al., 1997). Given that potentiometric

82   titrations have tentatively identified surface functional groups with different pKa values (Fein

83   et al., 1997; Small et al., 1999; Haas et al., 2001; Yee and Fein, 2001; Martinez et al., 2002;

84   Phoenix et al., 2002; Ngwenya et al., 2003; Borrok et al., 2005; Dittrich & Sibler, 2006;

85   Gélabert et al. 2006; Guiné et al., 2006; Guiné et al., 2007; Ojeda et al., 2008; Tourney et al.,

86   2008, Lalonde et al., 2008; Pokrovsky et al., 2008), including acidic (carboxyl groups),

87   neutral (phosphate groups) and basic (hydroxyl/amine groups), surface complexation models

88   suggested that metal adsorption at acidic and circum-neutral pH occurred predominantly to

89   carboxyl groups.

90   Three subsequent developments cast doubt on this assumption. (i) Fowle et al (2000)

91   reported significant uranyl (UO_2^{2+}) adsorption onto *Bacillus subtilis* at very low pH, which

92   could only be successfully modelled assuming adsorption to undeprotonated phosphate sites.

93   This was later confirmed by X-ray adsorption spectroscopy (XAS) experiments by Kelly et al

94   (2002). (ii) Through a rigorous mathematical description of ferrous iron adsorption to *B.*

95   *subtilis*, Châtellier and Fortin (2004) showed that metal adsorption commences well before

96   sites start to de-protonate, and that even at low pH, adsorption appeared to occur

97   predominantly to neutral pK$_a$ sites. (iii) Further XAS experiments by Boyanov et al (2003)

98   revealed that at low pH, Cd^{2+} adsorption occurred to phosphate sites, as opposed to carboxyl

99   sites postulated by Fein et al (1997). What emerged from these observations was that surface

100   complexation models provided only circumstantial evidence of the adsorption stoichiometry

101   but that a detailed understanding of the binding mechanism required spectroscopic

102   confirmation (Kelly et al., 2002). Nevertheless, stability constants derived from surface

103 complexation models have been used to predict metal mobility in porous media (Yee & Fein,

104 2002; Turner & Fein, 2007) and biofilms (Phoenix & Holmes, 2008) with reasonable success.

105   In the last decade or so, the biogeochemical behaviour of lanthanides has received

106 increasing attention. One reason for this emphasis is that lanthanides have been used as

107 fertilisers for over 20 years, in East Asia at least (Tyler, 2004). Although their toxicity in such

108 systems is unknown, they provide possible analogues for studying the physiological uptake

109 mechanisms of similarly charged (trivalent) toxic metals such as Al (Bennet & Green, 1992;

110 Ishikawa et al., 1996; Ding et al., 2005), which are often difficult to study because of their

111 low solubility under natural pH conditions. Some lanthanides are also by-products of the

112 nuclear fuel cycle, and the similarity in valence to some of the actinides makes them good

113 analogues for understanding the behaviour of these more problematic elements (Markai et al.,

114 2003). If studied as a suite, lanthanide fractionation patterns make them important indicators

115 of geochemical processes (Henderson, 1984), and have recently been suggested as potential

116 bio-signatures owing to unique fractionation patterns that develop in contact with biological

117 surfaces (Takahashi et al., 2005; Takahashi et al., 2007).

118   Unlike the common trace metals, however, relatively fewer studies have examined the

119 adsorption of lanthanides by microbes. Among the early reports on selected lanthanides, there

120 was an overwhelming view that lanthanide interaction with bacteria occurred predominantly

121 via surface adsorption, postulating adsorption to carboxyl sites as the main mechanism (e.g.

122 Bayer & Bayer, 1991; Andres et al., 1993; Texier et al., 1999; Philip et al., 2000; Texier et

123 al., 2000). More recently, Fein et al (2001) calculated a log K of 5.1±0.2 for monodentate Nd

124 adsorption to carboxyl sites on *Bacillus subtilis* cells. By comparison, Markai et al (2003)

125 used time-resolved laser-induced fluorescence spectroscopy to identify surface sites

126 responsible for Eu adsorption to *Bacillus subtilis*. The spectroscopic measurements suggested

127 carboxyl complexation at low pH, with minor contribution from phosphate sites at circum-

128 neutral pH. Similar techniques, applied to the adsorption of Eu to three different gram-

129 negative bacteria by Ozaki et al (2005), revealed differences in the coordination environment

130 of Eu among strains, suggesting that coordination may depend on fine scale differences in

131 cell surface chemistry. Lastly, using distribution coefficients for the simultaneous adsorption

132 of 15 lanthanides, Takahashi et al (2005) have postulated that adsorption is likely to occur

133 predominantly to phosphate groups at low pH, with carboxyl sites only coming into play at

134 low biomass concentrations. The selective adsorption of the heavy rare earth elements

135 (HREE) by phosphate sites was invoked to explain the extreme HREE-enrichment observed

136 at high biomass concentrations, based on pattern matching using phosphate-containing

137 ligands.

138   The objective of this study was to attempt a consistent model of lanthanide adsorption on

139 bacterial cell surfaces using selected elements representing light (Lanthanum and

140 Neodymium), middle (Samarium and Gadolinium) and heavy (Erbium and Ytterbium)

141 lanthanides. Macroscopic adsorption and surface complexation modelling of the adsorption

142 data is combined with X-ray absorption spectroscopic measurements in order to calculate

143 site-specific surface complexation constants for lanthanide adsorption, and to identify

144 adsorption sites on cell surfaces. Several studies have used time-resolved laser-induced

145 fluorescence spectroscopy (Texier et al., 2000; Markai et al., 2003; Ozaki et al., 2005)) to

146 study lanthanide adsorption to bacterial surfaces. However, to our knowledge, no previous

147 study has employed XAS to investigate adsorption of lanthanides to bacterial cells.

148

149   **2 Experimental Methods**

150 **2.1   Biomass preparation**

151 A copper-resistant strain of gram-negative *Pantoea agglomerans* (formerly identified to

152 genus level as belonging to *Enterobacteriacea,* Ngwenya et al., 2003*)* was grown for 24

153 hours in 2L flasks containing 1L of media made with 30g/L tryptone soya broth and 0.5%

154 yeast extract. The bacteria were harvested by centrifugation for 20 minutes at 23,420 x g and

155 4°C. The cells were re-suspended in 1L of de-ionised water and stirred at 4°C for about 20

156 minutes on a magnetic stirrer. This process was repeated three times, after which cells were

157 frozen overnight and then freeze-dried to yield a dry powder that was used in the

158 experiments. Although this approach is different from similar metal-bacteria adsorption

159 studies which use fresh cells, our ultimate objective is to study the whole suite of lanthanides

160 (plus Y), using the same batch of cells, in order to avoid inter-culture variability reported in

161 these other studies (e.g. Heinrich et al., 2007). Viability tests using LIVE/DEAD BacLight[TM]

162 molecular probes have shown most of the cells (>90%) to be viable after this treatment.

163

164 **2.2 Adsorption Edge Experiments**

165 Sorption experiments were conducted as a function of pH using suspensions of the bacteria in

166 0.01M $NaClO_4$ electrolyte in acid-cleaned, 50 ml polycarbonate centrifuge tubes. A stock

167 suspension was made from the lyophilised cells by first re-hydrating the cells for 1 hour in

168 0.01M $NaClO_4$ at 4°C. Cells were then rinsed in the electrolyte three times, each followed by

169 centrifugation at 17,210 x g for 10 minutes. After the final rinse, electrolyte was added to

170 dilute the cell suspension to the desired concentration, followed by addition of metal from

171 1000 mg/L stock solutions in 1% HNO_3. The pH of this stock suspension was then adjusted

172 upward in ~0.25 pH steps whilst continuously purging the headspace with N_2 to avoid

173 dissolution of CO_2 and potential precipitation of carbonates. At each pH, from 2.5 upwards,

174 20 ml was transferred into a 50 ml polycarbonate centrifuge tube and equilibrated for 3 hours

175 on a carousel rotating at 30 revolutions per minute. Two 5 ml sub-samples were transferred

176 into pre-weighed glass vials and evaporated to constant weight in order to determine the exact

177 biomass concentration, after correcting for a 5 ml electrolyte blank. Suspension pH was

178   measured at room temperature (23±1 °C) using a glass combination electrode connected to a

179   Hanna Instrument HI 9025 pH/Eh meter after a 3-point calibration using Merck buffers of

180   4.00, 7.00 and 9.22. Although the background electrolyte (0.01 M) is within the range of

181   NBS buffers (~0.1 M), we tested the response of the pH probe by checking the calibration

182   against a pH 4.00 buffer made in 0.01M NaClO4 instead of ultrapure water, and recorded a

183   pH of 3.99±0.01. Furthermore a 10^{-3} M HCl solution diluted from a 1 M volumetric standard

184   gave a pH of 3.01±0.02.

185   The above equilibration time was chosen based on preliminary kinetic experiments which

186   showed attainment of constant adsorption and suspension pH between 1 and 3 hours.

187   Furthermore, the upward-pH adjustment was adopted because previous experiments with this

188   strain have shown that it can produce soluble organics around circum-neutral pH values

189   (Ngwenya et al., 2003; Ngwenya, 2007), which are likely to decrease sorption density, as also

190   observed for *Bacillus subtilis* by Takahashi et al (2005). Nevertheless, a reversibility test was

191   performed based on a modification of the method of Fowle and Fein (1999), in which a

192   parent suspension spiked with Er was split into equal volumes to ensure the biomass and

193   initial metal concentrations were the same. One half was equilibrated at pH 2.5 for 3 hours,

194   then adjusted upwards in roughly 0.25 pH steps, with sub-sampling (20 ml) followed by

195   further equilibration for 3 hours. The second half was initially equilibrated at pH 6.5, then

196   adjusted downwards and re-equilibrated for a further 3 hours.

197   For four of the six lanthanides (La, Nd, Sm and Yb), two experiments, each with a

198   different biomass and initial metal concentration, were carried out. We present data for

199   suspensions using nominally ~0.2 g/L biomass with both 2 mg/L and 4 mg/L initial

200   lanthanide concentrations. Details of individual experiments are given in Table 1.

201   Calculations using MINTEQA2 (Allison et al., 1991) and first hydrolysis constants from

202   Klungness and Byrne (2004) and from Smith & Martell (1976) showed that at these

203 concentrations, metal hydroxides do not precipitate out at the target pH values. However,

204 controls (metal without biomass) showed that as much as 20% of each metal was potentially

205 adsorbed to containers around pH 7. No adsorption to containers was observed at pH values

206 below 5.5 but we often detected around 3% adsorption around pH 6, increasing to about 7%

207 by pH 6.5. We tested these observations using Teflon centrifuge tubes and measured similar

208 adsorption. Thus our experiments were restricted to pH ≤ 6.5, where speciation calculations

209 showed that between 97% (Yb) and 99% (La) of the lanthanide was in the form of the

210 hydrated trivalent ion and the rest as $LnOH^{2+}$. Nevertheless, we are confident that the error

211 introduced by this artefact on the experimental data is small given the stronger adsorption to

212 cells, especially as initial addition of the lanthanide was done at low pH. Sampling involved

213 pelleting (17,210 x g) the cells and filtering 10 ml of the supernatant into an acid-cleaned

214 bottle. These solutions were acidified to 2% v/v HNO_3 and stored at 4°C before metal

215 analysis by ICP-MS using matrix-matched standards. The use of freeze-dried cells can affect

216 total metal adsorbed, as demonstrated recently by Gabr et al. (2008). Thus, a further

217 adsorption edge experiment was carried out to compare fresh and freeze-dried cells, using the

218 element Nd, and similar biomass concentrations (0.21±0.01 g/L).

219 For the analysis, our sample solutions were diluted 1000 fold with 5% HNO_3, and metal

220 concentration was determined using a VG Elemental PlasmaQuad II+ Quadrupole mass

221 spectrometer at the Scottish Universities Environmental Research Centre (SUERC). The

222 metal concentration in the solution was obtained by reference to a calibration line produced

223 by the analysis of standard solutions containing known concentrations of the element. Each

224 sample value was corrected for procedural blank containing ultrapure water and 5% HNO_3.

225 Indium, Rhenium, and Ruthenium were selected as internal standards to monitor the

226 condition of the VG PQII+ within each session. The accuracy of the procedure was measured

227 by including an international environmental reference material BCR-1 (Govindaraju, 1984).

228   Although BCR-1 is not representative of the sample matrix, its light REE enrichment is ideal

229   for assessing the stability of the ICP on the day of the analysis to minimise interferences and

230   monitor changes during the analysis. Isotope peaks were determined in peak jumping mode

231   with 3 points per peak using three 60s integrations. When available, multiple isotopes were

232   selected for each element and the values averaged. Thus we used the following isotopes for

233   each element: La (^{139}La), Nd (^{145}Nd and ^{146}Nd), Sm (^{147}Sm, ^{149}Sm, and ^{152}Sm), Gd (^{155}Gd and

234   ^{157}Gd), Er (^{166}Er and ^{168}Er) and Yb (^{172}Yb, 1^{73}Yb and ^{174}Yb). Isotopes free from interference

235   (oxide or isobaric) were selected. Such care was necessary because some samples were

236   analysed alongside solutions containing mixtures of lanthanides, results of which will be

237   published elsewhere (Ngwenya et al., 2009). As a precaution against high Ba blanks, we also

238   routinely check for Ba oxide interference even during individual lanthanide analysis. The

239   average value of 3 biomass free controls over the range pH 2-4 (to ensure no adsorption to

240   containers walls) was used to determine the true starting concentration, which is given in

241   Table 1. Precision of sample preparation was monitored by analysing 3 duplicate pH values

242   and differences were smaller than 10%.

243

244   **2.3   Data Analysis**

245   Metal adsorption was calculated by mass balance from the difference between initial

246   concentration and the amount in solution after equilibration. The resulting adsorption edges

247   were modelled using the FITEQL 4 optimisation routine (Herbelin & Westall, 1999) to

248   determine intrinsic metal-site stability constants, using the weighted sum of squares

249   normalised by the number of degrees of freedom (*WSOS/DF*) to select the best-fitting model.

250   Values between 0.1 and 20 are normally considered good fits (Herbelin and Westall, 1999).

251   A constant capacitance electric field model with activity correction was used, with the same

252   surface area ($140 m^2/g$), capacitance ($8 F/m^2$), deprotonation constants and surface site

253 densities as in Ngwenya et al (2003). Despite its limitations, the constant capacitance model

254 was preferred over more recent, non-electrostatic approaches (e.g. Fein et al., 2005; Borrok et

255 al., 2005) because of the high lanthanide valence (Marmier & Fromage, 1999), and because

256 attempts with non-electrostatic models did not always produce consistent results between

257 different lanthanide to biomass ratios. Acid-base equilibria for the electrolyte and water were

258 included in the equilibrium problem, including lanthanide hydrolysis reactions whose

259 stability constants were taken from Klungness and Byrne (2000).

260

261 **2.4   Samples and standards for X-Ray Absorption Spectroscopy**

262 Based on the fact that adsorption density of cations increases with pH and previous studies

263 have shown that the coordination environment can vary depending on adsorption density (e.g.

264 Kelly et al., 2002; Boyanov et al., 2003; Guiné et al., 2006), it was necessary to analyse

265 biomass samples at low and high (circum-neutral) pH in order to examine speciation at low

266 and high adsorption densities. Our experiments were focussed on four of the six lanthanides

267 (Nd, Sm, Er and Yb), again chosen to represent light, middle and heavy lanthanides, and with

268 biomass samples (0.2g/L and metal concentrations of 4 mg/L) adjusted to pH 3.5 and 6. After

269 equilibration for 3 hours, the suspension was centrifuged at 23,420 x g for 20 minutes,

270 followed by a quick rinse in pH-adjusted 0.01M NaClO4 electrolyte and further

271 centrifugation to remove un-adsorbed metal. The resulting biomass paste was loaded onto

272 slots in Al plates to a thickness of 1mm, covered with Kapton tape and stored at -80°C until

273 analysis. For Sm and Yb, we also tested their coordination environment at a higher biomass

274 (1g/L) with 10 mg/L initial metal concentration to examine if the coordination changed when

275 each of the different surface sites were slightly in excess to probe possible site selectivity.   In

276 order to validate our analysis methods reference solution standards of perchlorate, acetate,

277 citrate and glycerol-2-phosphate were analysed, and these gave broadly similar results to

278 biomass samples in terms of bond distances.

279

280

281 **2.5   X-Ray Absorption Spectroscopy measurements and data analysis**

282 X-ray absorption spectra were collected in fluorescence mode on Stations 7.1 and 16.5 of the

283 SRS, Daresbury Laboratory. Both beamlines were operating with sagittally focussing double

284 crystal monochromators. Station 7.1 had a Si (111) set of crystals and a 9 element monolithic

285 Ge solid state detector. Station 16.5 had a Si (220) set of crystals and a 30 element Ge

286 detector. Data from the Nd and Sm (4 mg/L) samples were collected on station 7.1, whilst the

287 Yb, Er and the rest of the Sm data was collected on station 16.5. All the spectra were of the

288 L3 edge except for Er, where the L2 edge was used. The biomass samples were at 80K when

289 the data was collected to minimise any possible beam damage. There was no noticeable

290 difference in the XANES between the first and last scan of each biomass sample, showing

291 that the samples were unaffected by any short-lived beam damage. Up to 32 scans were

292 recorded and averaged for each biomass sample. The monochromator was calibrated using

293 appropriate metal foils, Ti, Mn, Fe and Cu.

294   The spectra were reduced using the programs EXCALIB, EXBROOK and EXSPLINE

295 (Ellis, 1995). The EXAFS was analysed in the program DL-EXCURVE (Tomic et al., 2005).

296 Data were fitted using *ab initio* phaseshifts calculated using Hedin-Lundqvist exchange and

297 Von Barth ground state potentials and single scattering using rapid curved wave theory. The

298 E_0, interatomic distances, number of atoms in each scattering shell (to the nearest integer) and

299 associated Debye-Waller factors (a measure of the static and thermal disorder in the distance)

300 data were minimised using the fit index R, defined as follows:

301          $R = \Sigma_i [(1/(\sigma_i))(|\text{experiment}(i) - \text{theory}(i)|] .100\%$ (1)

302 where:

303 $$1/(\sigma_i) = [k(i)]^3/(\Sigma_i[k(i)]^3 \,|experiment(i)|) \qquad (2)$$

304
305   In each case *ab initio* modelling of the data began with fitting the first coordination sphere

306 with oxygen and then attempts were made to fit further coordination shells of either

307 phosphorus or carbon. The fits for carbon and phosphorus were compared. Further to this a fit

308 was attempted using a second coordination sphere of both carbon and phosphorus. In order to

309 reduce the number of refined variables in modelling the second coordination sphere, initially

310 the shell occupancy number was fixed at half the value of the shell occupancy number for the

311 oxygen shell; once a bonding mode had been established this number was refined to the

312 nearest half integral value. The second sphere data is only considered valid where a 10%

313 improvement in the fit index is seen on addition of this shell. In differentiating between C and

314 P in this second sphere, we believe where the C or P model has a 5 % lower fit index than

315 the other, this model is definitely the preferred one according to the EXAFS, and is

316 consequently the model shown in the results table. The data quality and number of free

317 parameters mean that a model with a mixed second coordination sphere of C and P is not

318 justified statistically, though the EXAFS cannot rule out a component of carbonate or

319 phosphate bonding being present in samples where the other is the dominant mode.

320
321   3 Results and Discussion
322
323 3.1   Kinetics, reversibility and biomass preparation

324   Our time course experiments, conducted using Gd at pH around 4, showed that lanthanide

325 adsorption to the biomass was rapid, with approximately 99% of the 4 mg/L Gd adsorbed

326 within 5 minutes of contact. As shown in Figure 1a, however, the pH of the suspension rose

327 gradually during the first 100 minutes or so and only attained constancy thereafter. It was for

328 this reason that we chose (a) an equilibration time of 3 hours for our adsorption edge

329 experiments and (b) present our adsorption edge data as a function of final pH below.

330   Figure 1b shows that after this 3-hour equilibration, the adsorption reaction is also

331   completely reversible, as exemplified by the adsorption of 4 mg/L Er. Although individual

332   suspensions equilibrate to slightly differing final pH values, the two curves overlie each

333   other, clearly demonstrating equilibrium thermodynamic attainment. Figure 1c shows further

334   that by combining this data with that obtained on a different, independent suspension yields

335   excellent reproducibility.

336   Finally, a recent study by Gabr et al (2008) has shown that the amount of Pb and Ni

337   adsorbed by a strain of *Pseudomonas aeruginosa* was slightly higher when freeze-dried cells

338   were used instead of freshly prepared cells. We tested this with our *Pantoea agglomerans*

339   strain using 2 mg/L Nd and found no differences in adsorption density between fresh and

340   freeze-dried cells (Fig. 1d), both in terms of adsorption edges and modelled stability

341   constants.

342

343   **3.2   Macroscopic adsorption and surface complexation modelling**

344   Macroscopic adsorption experiments were designed to provide information on what type

345   of sites are involved in lanthanide uptake under the limited range of acidic pH conditions

346   tested. The experiments were focussed on pH-dependent adsorption because it has been

347   established that such experiments provide ideal data to quantify the stability constants

348   between each metal and the sites involved, although adsorption isotherm experiments are also

349   useful confirmatory tools. Results from these experiments are shown in Figure 2, where the

350   percentage of metal adsorbed is plotted against final suspension pH, and curves represent

351   different model fits to the data. In all cases, the amount of lanthanide adsorbed increases with

352   increasing pH, consistent with the expected behaviour for cationic adsorbents.

353   Considering that kinetic and reversibility experiments indicated attainment of equilibrium,

354   mass balance constraints on the total concentration of each metal should show an increase in

355 percent lanthanide adsorbed with decreasing initial metal (4 mg/L to 2 mg/L) to biomass

356 ratio. This behaviour is clearly evident in the Sm and Yb adsorption edges. In contrast, the La

357 and Nd edges are practically identical. We found that the biomass concentration in the 2

358 mg/L La experiment was much lower than the nominal 0.2 g/L, being about 0.12 g (due to

359 losses during washing), resulting in a higher metal to biomass ratio for this suspension.

360 Equally, the measured starting biomass concentration for 4mg/L Nd was 0.25 g/L explaining

361 the higher percentage adsorption in this experiment. To illustrate this further, we calculated

362 *relative* metal to biomass concentrations between the 4 mg/L and the 2 mg/L suspensions in

363 our study, by dividing the lanthanide to biomass ratio for the 4 mg/L experiment by the

364 corresponding ratio in the 2 mg/L experiment. This revealed that by using similar mg/L

365 instead of equimolar concentrations, the relative metal to biomass ratio increased with

366 increasing atomic number. What emerges from this inadvertent approach is that relative

367 ratios below about 1.5 are not able to resolve the two adsorption edges, being within the error

368 scatter of the data.

369 Similarly, comparison amongst the elements using adsorption at 50% does not show

370 systematic variation with atomic number. For the 4 mg/L suspensions, where the biomass

371 concentrations are closer to each other, we find that 50% adsorption occurs above pH 4 for

372 both La and Nd and below pH 4 for Sm, Gd, Er and Yb, suggesting that middle and heavy

373 lanthanides sorb more strongly to the biomass. Surface complexation modelling is therefore

374 critical to confirm that the mass balance constraints on biomass are applicable, as well as to

375 confirm the relative adsorptive strength of the 6 elements.

376 Modelling was set with the following generic reaction stoichiometry:

377 $$ROH_n^{n-1} + Ln^{3+} \Leftrightarrow (LnROH_n)^{(n+2)+} \tag{3}$$

378   where ROH_n represents a protonated surface functional group, Ln^{3+} is the lanthanide cation

379   and n represents the number of protons attached to the surface functional group. For the

380   constant capacitance electrostatic model, we define an intrinsic stability constant ($K_{int.}$), thus:

381
$$K_{int} = \frac{\left|(LnROH_n)^{(n+2)}\right|}{\left[ROH_n^{n-1}\right]\left[Ln^{3+}\right]} e^{((F\psi/RT)(n+2))} \qquad (4)$$

382   where F is the Faraday constant, ψ is the potential at the cell surface, R is the universal gas

383   constant and T is temperature. The following stoichiometries were tested:

384     $ROH + Ln^{3+} \Leftrightarrow Ln(ROH)^{3+}$, $n=1$.   (5)

385     $RO^- + Ln^{3+} \Leftrightarrow Ln(RO)^{2+}$, $n = 0$.   (6)
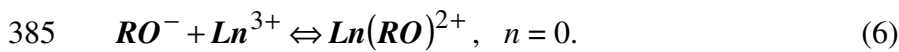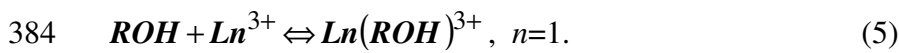
386   Reactions 5 and 6 are essentially regarded as representing outer-sphere and inner-sphere

387   complexation respectively (Langmuir, 1997). Deprotonation constants and site densities

388   determined from acid-base titrations by Ngwenya et al (2003) were used as input in metal

389   adsorption models. Other thermodynamic parameters were obtained from Smith & Martell,

390   (1976) and from Klungness & Byrne (2000). The WSOS/DF calculated by FITEQL was used

391   to select the best-fitting model, in conjunction with visual adherence of the model curves to

392   the experimental data. Reaction (5) was tested, either alone or in combination with reaction

393   (6), because of previous findings suggesting the involvement of neutral surface sites for high

394   valance cations such as UO_2^{2+} (Fowle et al., 2000, Haas et al., 2001). However, both

395   approaches invariably resulted in much higher WSOS/DF values. Other stoichiometries (e.g.

396   bidentate) were tested with similar negative outcomes. Thus, the modelling results collated in

397   Table 2 represent best-fitting stability constants based on reaction (6).

398   For La, lower WSOS/DF values were associated with deprotonation constants tentatively

399   ascribed to phosphate sites at both metal to biomass ratios. The difference in WSOS/DF

400   values between adsorption to carboxyl and phosphate sites is higher for the 4 mg/L dataset

401   than the 2 mg/L dataset, where these values are practically indistinguishable. Nevertheless, a

402 forward modelling of the adsorption isotherm using the mean pK values shows clearly that

403 both datasets are optimally fit with the phosphate surface complex (Fig. 2a), although

404 carboxyl complexation appears to be equally reasonable at low pH. Attempts to reproduce the

405 adsorption data with a forward model involving simultaneous adsorption to carboxyl and

406 phosphate sites overestimated the adsorption density across the whole range of pH.

407   Modelling of the Nd data was consistent between the two metal/biomass ratios in yielding

408 a lower WSOS/DF value for carboxyl adsorption. However, the WSOS/DF value for

409 carboxyl complexation in the 2 mg/L dataset was well below the acceptable value of 0.1,

410 apparently suggesting that the model contains too many adjustable parameters or that the

411 error estimates are too large (Herbelin & Westall, 1999). By comparison, the WSOS/DF

412 value for phosphate adsorption was more reasonable at 0.32. As can be seen in Figure 2b,

413 mean phosphate complexation constants perform marginally better in predicting the measured

414 adsorption edges, particularly at the lower pH end. Interestingly, Fein et al (2001) calculated

415 a Log K of 5.1±0.2 for monodentate Nd adsorption to carboxyl sites on *Bacillus subtilis*. Our

416 Nd value of 5.06±0.1 is therefore practically identical to their value. No comparison can be

417 made for phosphate complexation as Fein et al (2001) did not report a stability constant for

418 this reaction.

419   Sm models yielded lower WSOS/DF values whenever carboxyl surface parameters were

420 used. However, differences in WSOS/DF values were very small and the phosphate model

421 parameters were just as tightly constrained. As shown in Figure 2c, mean carboxyl and

422 phosphate stability constants provide reasonable reproduction of the adsorption edges. Subtle

423 differences are evident at low pH where carboxyl models perform better but the phosphate

424 site performs marginally better at pH values above 4.5. The single metal to biomass data that

425 we have for Gd suggests adsorption to phosphate sites performs slightly better (Fig. 2d).

16

426   Carboxyl models appear to provide better fits to all the 4ppm Er data than phosphate

427   models (Fig. 2e). Similarly, lower WSOS/DF values were associated with Yb adsorption to

428   carboxyl sites for both the 2 mg/L and 4 mg/L data (Fig. 2f). This is also reflected in the

429   slightly better fit to the adsorption data using carboxyl models, although the phosphate site

430   predicts the data slightly better at low pH in the 2 mg/L data.

431   In summary, it appears that lanthanide adsorption edges below pH 6.5 are consistent with

432   adsorption to phosphate groups for both of the light lanthanides examined in this study. By

433   contrast, the two middle lanthanides (Sm and Gd) are not consistent, with Sm apparently

434   preferring carboxyl sites whereas Gd is best fit with phosphate sites, although the Gd

435   adsorption is less well constrained based on one metal to biomass dataset. In contrast, both of

436   the heavy lanthanides are best fit with carboxyl adsorption, although phosphate fits to the

437   data are also generally good. The phosphate predictions are indistinguishable from carboxyl

438   predictions within the error bounds found in most experiments of metal adsorption to bacteria

439   where biomass and/or metal concentration is varied (Fein et al., 1997; Daughney et al., 2001;

440   Haas et al., 2001; Martinez & Ferris., 2001; Ngwenya et al., 2003; Châtellier & Fortin, 2004;

441   Yee et al., 2004; Borrok et al., 2005; Toner et al., 2005; Pokrovsky et al., 2005; Gélabert et

442   al., 2006; Burnett et al., 2006). We conclude that surface complexation modelling of the

443   macroscopic adsorption data either points to the involvement of both sites or that it is simply

444   not able to reveal selectivity in surface speciation. One possible reason for this is that in all

445   our experiments, the concentration of each site in the suspension is in excess of the initial

446   total lanthanide concentration. Equally, the pH range of the data may be too narrow to resolve

447   between the different possible surface complexes. However, the measured adsorption does

448   not change above pH 6.5 so data beyond this pH does not yield additional information.

449   Attempts to use higher initial lanthanide concentrations (15ppm) were not useful as there was

450   some evidence of surface precipitation above pH 5 (data not shown).

3.3   Lanthanide coordination from EXAFS measurements

452

453   Attempts were made to obtain X-ray absorption spectra for Nd, Sm Yb and Er samples

454   with 4 mg/L initial metal concentration for both pH's (3.5 and 6). However, in the case of

455   Nd, the concentration of adsorbed metal in the pH 3.5 sample was not sufficient to give

456   analysable data. Data was collected out to 12 k ($\mathring{A}^{-1}$), but in most cases could only be

457   analysed to ca.10 k as beyond this point the signal-to-noise ratio is poor. This accounts for

458   the different data ranges in Figures 3 and 4. . In one Sm sample and Yb sample the analysis is

459   restricted to about 8 k because of Fe contamination in the cryosystem (Sm), and low data

460   quality for the Yb sample. The EXAFS analysis results are shown in Table 3.

461   In a previous study of Nd co-ordinated to alfalfa biomass, Parsons et al (2005) showed two

462   Nd-O first coordination sphere distances of around 2.38 and 2.56 Å. They attributed these to

463   water bound O (2.38Å) and surface bound O (2.56Å). Acetate or similar carboxylate groups

464   displayed an Nd-C distance of about 3.6 Å. In our modelling, attempts to split the oxygen

465   coordination shell led to very high correlations between the distances and Debye-Waller

466   factors, thus the shell has been left unsplit. At 3.92 Å, the Nd(-O-)P distance is too long for

467   bidentate phosphate coordination, but reasonable for monodentate phosphate bonding. This is

468   because in Nd-Monazite ($NdPO_{4)}$, the Nd-P distances are 3.15 and 3.25 Å for bidentate

469   phosphate and 3.47 and 3.73 Å for monodentate phosphate, with the Nd –O distances ranging

470   between 2.42 and 2.79 Å, with a mean of 2.52 Å (Ni et al, 1995). Our distance of 3.92 Å for

471   Nd-P is similar to that found in ultraphosphate and metaphosphate glasses (3.87 Å) by

472   Karabulut et al (2005). No Nd-C coordination was evident in the pH6, 4ppm biomass data.

473   We saw the most significant pH-dependant changes in the EXAFS for Samarium (Figure

474   3). At low pH (3.5) there are indications of monodentate phosphate binding at 3.86 Å,

475   comparable to the monodentate Sm-O-P of 3.63 -3.78 Å in $KSmHP_3O_{10}$ (Zouari *et al.*, 2000).

476　The pH 6 sample shows carbon in the second coordination sphere. In the 10 mg/L sample this

477　shell is quite distinct at 3.48 Å, similar to a monodentate Sm(-O-)C of 3.47 Å in Samarium

478　Carbonate Hydroxide (Xu *et al.*, 2006). In the 4 mg/L pH 6 sample the carbon shell does

479　not fit the Fourier Transform well (Figure 3), though it improves the EXAFS fit. The

480　amplitude of this oscillation is also quite low compared to the other Sm second shell EXAFS

481　(Figure 3). Further the Sm-C distance is quite different and a little longer than expected (3.64

482　Å), thus this may be indicative of mixed speciation in this sample, where more than one

483　bonding mode exists in substantial fraction and thus the bare two shell fit is unrepresentative

484　- the EXAFS being washed out by destructive interference. **T**hus we believe the binding

485　mode may actually be a mixture of phosphate and carboxyl in this sample. It seems therefore

486　that when the biomass to Sm ratio is increased (1g/L, 10ppm) the carboxyl mode

487　predominates. These observations are entirely consistent and may suggest carboxyl site

488　preference by Sm.

489　For the higher lanthanides, Er and Yb, the EXAFS results (Figure 4) are similar with both

490　showing P in the second shell at distances 3.81-3.83 Å (Er) and 3.75-3.80 Å (Yb) similar to

491　monodentate phosphate bonding (Er –O-P 3.75 Å, Yb- O –P 3.72 Å in LnPO4 (Milligan and

492　Mullica, 1983) . This distance would need to be *ca*. 0.4 Å less for bidentate coordination. No

493　C in the second coordination sphere could be fitted convincingly for any of these datasets,

494　however examination of the individual shell EXAFS contributions (Figure 4) and Fourier

495　transforms (Figure 4) reveals again that for the pH 6 samples the P shell amplitude is smaller,

496　and also the shell occupancy numbers for the Yb pH 6 P shells are lower than for the pH 3.5

497　samples. These related observations are both indicative that, in the higher pH bonding,

498　monodentate phosphate coordination may not be the whole story; however, our analysis of

499　the EXAFS data for the Er and Yb does not allow us to say whether this is due to some

500　carboxyl bonding or other coordination mode.

501   In the EXAFS the lanthanide contraction is noticeable with the Ln – O distance gradually

502   decreasing from 2.48 – 2.45 – 2.33 – 2.28 from Nd to Sm to Er to Yb. Also the Er appears to

503   have slightly fewer oxygen atoms around it than the other lanthanides. The coordination

504   number of oxygen atoms in the first shell is similar for all the atoms, refining to values

505   between 7.5 and 10.5.

506   Our spectroscopic findings are consistent with other EXAFS studies in two respects.

507   Firstly, they show the predominance of phosphate binding at low pH, as previously reported

508   for uranyl and Cd adsorption to *Bacillus subtilis* by Kelly et al (2002) and Boyanov et al.

509   (2003) respectively. Secondly, they show that as the pH increases at a constant biomass

510   concentration, the carboxyl group starts to get involved in lanthanide bonding. Thus, in

511   summary the EXAFS analysis is strongly indicative of monodentate phosphate coordination

512   at low pH for the 4 lanthanides studied by XAFS here, whereas at higher pH, phosphate

513   coordination dominates for Nd, Er and Yb, whereas carboxyl coordination dominates for Sm.

514   However the data indicates that for the heavy lanthanides, there may well be more than one

515   bonding mode present.

516

517   **3.4   General synthesis**

518   This study combined surface complexation modelling of macroscopic adsorption data with

519   X-ray spectroscopic measurements to identify lanthanide sorption sites on the bacterial

520   surface. The experiments were limited to the acidic region of the pH spectrum because nearly

521   100% adsorption was attained above pH 5 for the range of metal to biomass ratios used. As a

522   result, surface complexation modelling was focussed on sites that deprotonate in this pH

523   range, and suggested that there may be variations in the dominant sorption sites across the

524   lanthanide series. Specifically, the adsorption of both of the light lanthanides was best

525   modelled assuming adsorption to phosphate sites. However, the rest of the lanthanides could

526   be modelled equally well with carboxyl or phosphate sites, although Samarium was better

527   modelled with carboxyl relative to phosphate sites. Nevertheless, the differences in

528   performance between the two models were generally small, suggesting that surface

529   complexation modelling does not adequately discriminate between the two models. Lastly,

530   we found that for all the lanthanides, inner-sphere (proton exchange) complexation was the

531   most likely reaction stoichiometry, although this needs to be confirmed by conducting ionic

532   strength-dependent metal adsorption experiments. By comparison, X-ray spectroscopic

533   analyses are more consistent with adsorption of most lanthanides to phosphate sites, at least

534   at low adsorption densities (at low pH), with secondary involvement of carboxyl sites at high

535   adsorption density (high pH). Furthermore, spectroscopic analysis suggests that the

536   coordination to phosphate sites is monodentate. Some indication of carboxyl dominance was

537   inferred for Sm in the high biomass sample.

538   Thus, the first conclusion that arises from this study is that surface complexation

539   modelling and spectroscopic analysis are broadly consistent in their information content with

540   regard to surface site identity and lanthanide coordination environment. Coordination of light

541   lanthanides to phosphate groups, as implied by both techniques, is consistent with the

542   findings of Merroun et al (2003) for La adsorption to *M. xanthus*. Such a model was also

543   suggested by Takahashi et al (2005) for all lanthanides adsorbed onto *B. subtilis*, although

544   their experiments were conducted only at low pH values, where recent spectroscopic studies

545   (Kelly et al., 2002; Boyanov et al., 2003) seem to indicate that metal coordination to

546   phosphate site is a common phenomenon. These studies have also indicated that with

547   increasing pH, carboxyl sites become more involved in the adsorption reaction, because

548   carboxyl sites start to deprotonate (Fowle et al., 2000; Kelly et al., 2002). Although we do not

549   report Eu adsorption in this study, the pH-dependent behaviour contrasts with the findings of

550   Markai et al (2003), that low pH adsorption of Eu was due to carboxyl complexation, based

551   on time resolved laser-induced fluorescence spectroscopy (TRLFS) measurements, with

552   phosphate groups only coming into play at high pH and/or adsorption density. Notably, the

553   coordination environment of lanthanides has also been found to vary between bacterial

554   species (Ozaki et al., 2005). Thus it is not possible categorically to generalise our

555   observations, indicating that further work is required to develop a better understanding of the

556   lanthanide coordination environment in biological materials. More importantly, our study

557   demonstrates clearly that neither technique is capable of providing unambiguous coordination

558   information for lanthanide adsorption. This clearly justifies the use of complimentary

559   techniques in metal adsorption studies.

560   Finally, we note that the best fitting model for adsorption to phosphate sites is

561   consistent with inner-sphere (reaction 6) complexation, with adsorption to undeprotonated

562   phosphate sites (reaction 5) yielding WSOS/DF values around 50, and is therefore unlike the

563   coordination environment of the uranyl ion (Fowle et al., 2000; Kelly et al., 2002). Within the

564   gram-negative cell wall, the only structural components containing phosphate groups in the

565   outer membrane are phospholipids and N-acetylglucosamine phosphate, a component of

566   Lipid A in the lipopolysaccharide membrane (Beveridge & Fyfe, 1985; Madigan et al., 2003;

567   Guiné et al., 2006). As shown in Figure 5, both molecules contain phosphoester bonds, with a

568   monophosphoester bond in N-acetylglucosamine-6-phosphate (Nishitani et al., 2006), and a

569   phosphodiester bond in phospholipids, typified here by phosphatidylethanolamine (Mayes,

570   1985).

571   Experimental studies of protonation reactions for phosphodiesters in aqueous solutions are

572   consistent with a pKa of about -0.7 for the single hydroxylated functional group (Azema et

573   al., 2005). Thus, this functional group is likely to be deprotonated both at physiological

574   conditions and across our experimental pH spectrum. As such, it may be responsible for the

575   observed low pH adsorption of the light lanthanides in this study, and could also explain the

576   apparent pH-independent adsorption of uranyl ions reported by Fowle et al (2000) at low pH.

577   However, our model outcomes were realised with a *p*Ka of 6.9 for phosphate groups

578   (Ngwenya et al., 2003), which is closer to the deprotonation constant for the second hydroxyl

579   group on phosphoric acid, (*p*Ka ~7). Attempts to model the data with a non-electrostatic

580   model, which yielded a phosphodiester pKa around 3.9 (based on 4 variable biomass

581   titrations) for *Pantoea agglomerans*, did not produce consistent results across different metal

582   to biomass ratios and the resulting WSOS/DF values were always higher. This leads us to

583   speculate that the second hydroxyl group on N-acetylglucosamine phosphate makes this a

584   more likely candidate for lanthanide binding on a gram-negative bacterium. It may be

585   considered analogous to methylphosphoric acid, which has a second *p*Ka around 6.3 (Saha et

586   al., 1996). Such a conjecture need not conflict with phosphate binding of cations on gram-

587   positive cell walls, where phosphate groups are dominated by phosphodiester linkages in

588   teichoic acids (Heinrich et al., 2007), because gram-positive cell walls also contain other

589   phosphate groups in addition to phosphodiester linkages.

590

591   # 4 Conclusions

592   The objective of this study was to combine surface complexation modelling of macroscopic

593   adsorption data with X-ray spectroscopic measurements to identify lanthanide sorption sites

594   on the bacterial surface. We have shown that surface complexation modelling and

595   spectroscopic analysis yield complimentary information on the coordination environment of

596   the light lanthanides. Surface complexation modelling was consistent with the light

597   lanthanides adsorbing to phosphate sites, whereas the adsorption of middle and heavy

598   lanthanides could be modelled equally well by carboxyl and phosphate sites. Moreover,

599   proton exchange is the most likely reaction stoichiometry. The existence of such mixed mode

600   coordination was also confirmed by EXAFS analyses, which was consistent with adsorption

601 to phosphate sites at low pH, with secondary involvement of carboxyl sites at high pH.

602 Importantly, however, neither surface complexation modelling nor EXAFS analysis gave the

603 whole picture alone, emphasising the importance of using complimentary techniques in

604 understanding sorption mechanisms. Apparently, coordination to phosphate sites is

605 monodentate, and occurs to phosphate sites around pKa ~7. Based on these observations, we

606 conjecture that the phosphate sites are located on N-acetylglucosamine phosphate, the most

607 likely polymer with potential phosphate sites that deprotonate around neutral pH.

608

617

618 **References**

619

620 Allison, J.D.; Brown, D.S.; Novo-Gradac, K.J. (1991) *MINTEQA2: a geochemical*

621   *assessment data base and test cases for environmental systems: Version 3.0 User's*

622   *Manual*. Report EPA/600/3-91/-21, Athens, GA..

623 Andres, Y., MacCordick, H.J. and Hubert, J-C. (1993). Adsorption of several actinides (Th,

624   U) and lanthanide (La, Eu, Yb) ions by Mycobacterium smegmatis. *Appl. Microbiol.*

625   *Biotechnol,* **39**, 413-417.

626   Azema, L., Ladame, S., Lapeyre, C., Zwick, A. and Lakhdar-Ghazal, F. (2005). Does

627   phosphoryl protonation occur in aqueous phosphoester solutions? *Spectrochim. Acta, Part*

628   *A* **62**, 287-292.

629   Bayer, M.E. and Bayer, M.H. (1991). Lanthanide accumulation in the periplasmic space of

630   Escherichia coli. *Brit. J. Bacteriol.* **173**, 141-149.

631   Bennet, R.J. and Green, C.M. (1992). The use of lanthanum to delineate aluminium signalling

632   mechanisms functioning in roots of *Zea mays*. *Environ. Exper. Bot.* **32**, 365-376.

633   Beveridge, T.J. and Fyfe, W.S (1985). Metal fixation by bacterial cell walls. *Can. J. Earth.*

634   *Sci.* **22**, 1893-1898.

635   Borrok, D., Fein, J.B. and Kulpa, C.F., (2005). Proton and Cd adsorption onto natural

636   bacterial consortia: Testing universal adsorption behaviour. *Geochem. Cosmochim. Acta*

637   **68**, 3231-3238

638   Boyanov, M.I., Kelly, S.D., Kemner, K.M., Bunker, B.A., Fein, J.B. and Fowle, D.A. (2003).

639   Adsorption of cadmium to Bacillus subtilis bacterial cell walls: A pH-dependent X-ray

640   absorption fine structure spectroscopy study. *Geochem. Cosmochim. Acta* **67**, 3299-3311.

641   Burnett, P.G., Daughney, C.J. and Peak, D. (2006). Cd adsorption onto *Anoxybacillus*

642   *flavithermus*: surface complexation modelling and spectroscopic investigations. *Geochim.*

643   *Cosmochim Acta* **70**, 5253-5269.

644   Châtellier, X. and Fortin, D. (2004). Adsorption of ferrous ions onto *Bacillus subtilis* cells,

645   *Chem. Geol.* **212,** 209–228

646   Daughney, C.J., Fein, J.B. and Fortin, D. (2001). The effect of growth phase on proton and

647   metal adsorption by *Bacillus subtilis. Geochim. Cosmochim. Acta* **65**, 1025-1035.

648   Daughney, C.J., Fein, J.B. and Yee, N. (1998). A comparison of the thermodynamics of metal

649   adsorption onto two gram-positive bacteria. *Chem. Geol.* **144**, 161-176.

650   Ding, S., Liang, T., Zhang, C., Yan, J. and Zhang, Z. (2005). Accumulation and fractionation

651   of rare earth elements (REEs) in wheat: controlled by phosphate precipitation, cell wall

652   adsorption and solution complexation. *J. Exper. Bot*. **56**, 2765-2775.

653   Dittrich, M. and Sibler, S. (2006). Influence of H^+ and calcium ions on the surface functional

654   groups of *Synechoccus* PCC 7942 cells. *Langmuir* **22**, 5435-5442.

655   Ellis P. (1995). EXSPLINE - a program for EXAFS background subtraction, Daresbury

656   Laboratory, 2000. Based on an original program, SPLINE, PhD Thesis, University of

657   Sydney.

658   Fein, J.B., Boily, J-F., Yee, N., Gorman- Lewis, D., Turner, B. (2005). Potentiometric

659   titrations of *Bacillus subtilis* cells to low pH and a comparison of modelling approaches.

660   *Geochim. Cosmochim. Acta* **69**, 1123- 1132.

661   Fein, J.B., Daughney, C.J., Yee, N. and Davis, T.A. (1997). A chemical equilibrium model of

662   metal adsorption onto bacterial surfaces. *Geochim. Cosmochim. Acta* **61**, 3319-3328.

663   Fein, J.B., Martin, A.M. and Wightman, P.G. (2001). Metal adsorption onto bacterial

664   surfaces: Development of a predictive approach. *Geochim. Cosmochim. Acta* **65**, 4267-

665   4273.

666   Fowle, D.A. and Fein, J.B. (1999). Competitive adsorption of metal cations onto two gram

667   positive bacteria: Testing the chemical equilibrium model. *Geochim. Cosmochim. Acta* **63**,

668   3059-3067.

669   Fowle, D.A., Fein, J.B. and Martin, A.M. (2000). Experimental study of uranyl adsorption

670   onto Bacillus subtilis. *Environ. Sci. Technol*., **34**, 3737-3741.

671   Gabr, R.M., Hassan, S.H.A. and Shoreit, A.A.M (2008). Biosorption of lead and nickel by

672   living and non-living cells of *Psedomonas aeruginosa ASU 6a*. *Int. Biodet. Biodeg*., **62**,

673   195-203.

674 Gélabert, A., Pokrovsky, O.S., Viers, J., Schott, J., Boudou, A. and Feurtet-Maze, A. (2006).

675   Interaction between zinc and freshwater and marine diatom species: Surface complexation

676   and Zn isotope fractionation. *Geochim. Cosmochim Acta* **70**, 839-857.

677 Govindaraju, K. (1984). Compilation of working values and sample description for 170

678   International References samples on mainly silicate rocks and minerals. Geostandards

679   Newsletter Special Volume VIII, 1-8.

680 Guiné, V., Martins, J.M.F., Causse, B., Durand, A., Gaudet, J.-P. and Spadini, L. (2007).

681   Effect of cultivation and experimental conditions on the surface reactivity of the metal-

682   resistant bacteria Cupriavidus metallidurans CH34 to protons, cadmium and zinc. *Chem.*

683   *Geol.,* **236**, 266-280.

684 Guiné, V., Spadini, L., Sarret, G., Muris, M., Delolme, C., Gaudet, J-P. and Martins, J.M.F.

685   (2006). Zinc sorption to three Gram-Negative bacteria: Combined titration, modelling, and

686   EXAFS study. *Environ. Sci. Technol.*, **40**; 1806-1813.

687 Haas, J.R., Dichristina, T.J. and Wade Jr. R. (2001). Thermodynamics of U(VI) sorption onto

688   *Shewanella putrefaciens. Chem. Geol,* **180**, 33-54.

689 Heinrich, H.T.M., Bremer, P.J., Daughney, C.J., McQuillan, A.J. (2007). Acid- base titrations

690   of functional groups on the surface of the thermophilic bacterium *Anoxybacillus*

691   *flavithermus*: Comparing a chemical equilibrium model with ATR-IR spectroscopic data.

692   *Langmuir* **23**, 2731- 2740.

693 Henderson, P. (1984). General geochemical properties and abundancies of the Rare Earth

694   Elements. In Henderson, P. (ed.). Rare Earth Element Geochemistry, Developments in

695   Geochemistry 2, 1-32, Elsevier, Amsterdam.

696 Herbelin, A.L. and Westall, J.C. (1999). *FITEQL 4.0: a computer program for determination*

697   *of chemical equilibrium constants from experimental data*; Report 99-01, Department of

698   Chemistry Oregon State University, Corvallis.

699   Ishikawa, S., Wagatsuma, T. and Ikarashi, T. (1996). Comparative toxicity of Al3+, Yb3+,

700   and La3+ to tip-root cells differing in tolerance to high Al^{3+} in terms of ionic potentials of

701   hydrated trivalent cations. *Soil Sci. Plant Nutr*. **42**, 613-625.

702   Karabulut, M., Metwalli, E., Wittenauer, A.K., Brow, R.K., Marasinghe, G.K., Booth, C.H.,

703   Bucher, J.J. and Shuh, D.K. (2005). An EXAFS investigation of rare-earth local

704   environment in ultrapotassic glasses. *J. Non-Crystall. Sol.*. **351**, 795-801.

705   Kelly, S.D., Kemner, K.M., Fein, J.B., Fowle, D.A., Boyanov, M.I., Bunker, B.A. and Yee,

706   N. (2002). X-ray adsorption fine structure determination of pH-dependent U-bacterial cell

707   wall interactions. *Geochim. Cosmochim. Acta*. **66**, 3855-3871.

708   Klungness, G.D. and Byrne, R.H. (2000). Comparative hydrolysis behaviour of rare earths

709   and yttrium: the influence of temperature and ionic strength. *Polyhedron* **19**, 99-107.

710   Lalonde, S.V., Smith, D.S., Owttrim, G.W. and Konhauser, K.O. (2008). Acid-base

711   properties of cyanobacterial surfaces I: Influences of growth phase and nitrogen

712   metabolism on cell surface reactivity. *Geochim. Cosmochim. Acta*., **72**, 1257-1268.

713   (16)   Langmuir, D. (1997) *Aqueous Environmental Geochemistry*, Prentice Hall, New

714   Jersey, 600 pp.

715   Madigan, M.T., Martinko, J.M. and Parker, J. (2003). <u>Brock Biology of Microorganisms</u>.

716   Prentice Hall, New Jersey, Tenth edition, 1019pp.

717   Markai, S., Andres, Y., Montavon, G. and Grambow, B. (2003). Study of the interaction

718   between europium (III) and Bacillus subtilis: fixation sites, biosorption modelling and

719   reversibility. *J. Colloid. Interf. Sci*. **262**, 351-361.

720   Marmier, N. and Fromage, F. (1999). Comparing electrostatic and noelectrostatic surface

721   complexation modelling of the sorption of lanthanum on hematite. *J. Colloid Interf. Sci*.,

722   **212**, 252-263.

723 Martinez, R.E. and Ferris, F.G., (2001). Chemical equilibrium modelling techniques for the

724 analysis of high resolution bacterial metal adsorption data. *J. Colloid Interf. Sci.*, **243**, 73-

725 80.

726 Martinez, R.E., Smith, D.S., Kulczycki, E., Ferris, F.G. (2002). Determination of Intrinsic

727 Bacterial Surface Acidity Constants using a Donnan Shell Model and a Continuous pK_a

728 Distribution Method. *J. Colloid Interf. Sci.*, **253**, 130- 139.

729 Mayes, P. (1985). Lipids. In: Martin, D.W., Mayes, P.A., Rodwell, V.W. and Grinner, D.K.

730 (ends), Harper's Review of Biochemistry, Lange Medical Publications, Los Angeles,

731 California, pp.14-31.

732 Merroun, M.L., Ben Chekrou, K., Arias, J.M., Gonzalez- Munoz, M.T. (2003). Lanthanum

733 fixation by *Myxococcus xanthus*: cellular location and extracellular polysaccharide

734 observation. *Chemosphere* **52**, 113- 120.

735 Milligan, W.O. and Mullica, D.F. (1983). Structures of $ErPO_4$, $TmPO_4$ and $YbPO_4$ (1983)

736 *Acta Crystall. C* **39,** 23-24.

737 Ngwenya, B.T. (2007). Enhanced adsorption of zinc is associated with aging and lysis of

738 bacterial cells in batch incubations. *Chemosphere* **67**, 1982-1992.

739 Ngwenya, B.T., Sutherland, I.W. and Kennedy, L. (2003). Comparison of the acid-base

740 behaviour and metal adsorption characteristics of a gram-negative bacteria with other

741 strains. *Appl. Geochem.* **18**, 527-538.

742 Ngwenya, B.T., Tourney, J., Magennis, M., Kapetas, L. and Olive, V. (2009). A surface

743 complexation framework for predicting water purification through metal biosorption.

744 *Desalination* (in press).

745 Ni, Y.-X., Hughes, J.M. and Mariano, A.N. (1995). Crystal chemistry of the monazite and

746 xenotime structures. *Amer. Mineral*. **80,** 21-26.

747   Nishitani, Y., Maruyama, D., Nonaka, T., Kita, A., Fukami, T.A., Mio, T., Yamada-Okabe,

748   H., Yamada-Okabe, T. and Miki, K. (2006). Crystal structure of N-acetylglucosamine-

749   phosphate mutase, a member of the α-$_D$-phosphexomutase superfamily, and its substrate

750   and product complexes. *J. Biol. Chem.* **281**, 19740-19747.

751   Ojeda, J.J., Romero-González, M.E., Bachmann, R.T., Edyvean, R.G.J. and Banwart, S.A.

752   (2008). Characterisation of the cell surface and cell wall chemistry of drinking water

753   bacteria by combining XPS, FTIR Spectroscopy, modelling and Potentiometric titrations.

754   *Langmuir* **24**, 4032-4040.

755   Ozaki, T., Kimura, T., Ohnuki, T. and Francis, A.J. (2005). Associations of Eu(III) with

756   gram-negative bacteria, Alcaligenes faecalis, Shewanella putrefaciens, and Paracoccus

757   denitrificans. *J. Nucl. Radiochem. Sci.* **6**, 73-76.

758   Parsons, J.G., Peralta-Videa, J.R., Tiermann, K.J., Saupe, G.B. and Gardea-Torresdey, J.L.

759   (2005). Use of chemical modifications and spectroscopic techniques to determine the

760   binding and coordination of gadolinium (III) and neodymium (III) ions by alfafa biomass.

761   *Talanta* **67**, 34-45.

762   Philip, L., Iyendar, L. and Vekobachar, C. (2000). Biosorption of U, La, Pr, Nd, Eu and Dy

763   by Pseudomonas aeruginosa. *J. Industr. Microbiol. Biotechnol.* **25**, 1-7.

764   Phoenix, V.R. and Holmes, W.M. (2008). Magnetic resonance imaging of structure,

765   diffusivity and copper immobilisation in a phototrophic biofilm. *Appl. Environ.*

766   *Microbiol.,* **74**, 4934-43.

767   Phoenix, V. R., Martinez, R. E., Konhauser, K. O. and Ferris, F. G. (2002). Characterization

768   and implications of the cell surface reactivity of Calothrix sp. Strain KC97. *Appl. Environ.*

769   *Microbiol,* **68**, 4827-4834.

770   Pokrovsky, O.S., Martinez, R.E., Golube, S.V., Kompantseva, E.I. and Shirokova, L.S.

771   (2008). Adsorption of metals and protons on Gloeocapsa sp. cyanobacteria: A surface

772   speciation approach. *Appl. Geochem.*, **23**, 2574-2588.

773   Pokrovsky, O.S., Pokrovski, G.S., Gélabert, A., Schott, J. and Boudou, A. (2005). Speciation

774   of Zn associated with diatoms using X-ray Absorption Spectroscopy. *Environ. Sci.*

775   *Technol.* **39**, 4490-4498.

776   Saha, A., Saha, N., Ji, L.-n., Zhao, J., Gregáň, F., Sagadi, A.A., Song, B. and Sigel, H.

777   (1996). Stability of metal ion complexes formed with methyl phosphate and hydrogen

778   phosphate. *J. Biol. Inorg. Chem.*, **1**, 231-238.

779   Small, T.D., Warren, L.A., Rodent, E.E. and Ferris, F.G. (1999). Sorption of strontium by

780   bacteria, Fe(III) oxide, and bacteria-Fe(III) oxide composites. *Environ. Sci. Technol.* **33**,

781   4465-4470.

782   Smith, R.M. & Martell, A.E. (1976). <u>Critical Stability constants. IV. Inorganic complexes</u>,

783   Plenum Press.

784   Takahashi, Y., Châtellier, H., Hattori, K.H., Kato, K. and Fortin, D. (2005). Adsorption of

785   rare earth elements onto bacterial cell walls and its implication for REE sorption onto

786   natural microbial mats. *Chem. Geol.* **219**, 53-67.

787   Takahashi, Y., Kirata, T., Shimizu, H., Ozaki, T. and Fortin, D. (2007). A rare earth element

788   signature of bacteria in natural waters. *Chem. Geol.*, **244**, 569-583.

789   Texier, A.C.; Andres, Y., Illemassene, M. and Le Cloirec, P. (2000). Characterisation of

790   lanthanide ion binding sites in the cell walls of Pseudomonas aeruginosa. *Environ. Sci.*

791   *Technol.* **34**, 610-615.

792   Texier, A.C.; Andres, Y & Le Cloirec, P. (1999). Selective biosorption of lanthanide (La, Eu,

793   Lu) ions by *Pseudomonas aeruginosa*. *Environ. Sci. Technol.* **33**, 489-495.

794   Tomic, S., Searle, B.G., Wander, A., Harrison, N.M., Dent, A.J., Mosselmans, J.F.W. and

795   Inglesfield, J.E. (2005). CCLRC Technical Report DL-TR-2005-001, ISSN 1362-0207.

796   Toner, B., Macau, A., Marcus, M.A., Millet, D.B. and Esposito, G. (2005). Zn sorption by a

797   bacterial biofilms. *Environ Sci Technol.* **39**, 8288–8294.

798   Tourney, J., Ngwenya, B.T., Mosselmans, J.F.W., Tetley, L. and Cowie, G.L. (2008). The

799   effect of extracellular polymers (EPS) on the proton adsorption characteristics of the

800   thermophile Bacillus licheniformis S-86. *Chem. Geol.*, **247**, 1-15.

801   Turner, B.F. and Fein, J.B. (2007). Appropriateness of equilibrium assumptions for

802   determining metal distribution and transport in bacteria-bearing porous media. *Chem.*

803   *Geol*. **242**, 40-50.

804   Tyler, G. (2004). Rare earth elements in soil and plant systems-A review. *Plant Soil*, **267**,

805   191-206.

806   Xu, Y.;Ding, S.-H.;Feng, W.-J.;Zhou, G.-P.;and Liu, Y.G. (2006). Samarium(III) carbonate

807   hydroxide *Acta Crystall. E , Struct. Rep. Online* **62,** i147-i149.

808   Yee, N. and Fein, J.B. (2001). Cd adsorption onto bacterial surfaces: A universal adsorption

809   edge? *Geochim. Cosmochim. Acta,* **65**, 2037-2042.

810   Yee, N. and Fein, J.B. (2002). Does metal adsorption onto bacterial surfaces inhibit or

811   enhance aqueous metal transport? Column and batch reactor experiments on Cd–*Bacillus*

812   *subtilis*–quartz systems. *Chem. Geol.*, **144**, 161-176.

813   Yee, N.; Benning, L. G.; Phoenix, V. R. and Ferris, F. G. (2004). Characterization of metal-

814   cyanobacteria sorption reactions: A combined macroscopic and Infrared spectroscopic

815   investigation. *Environ. Sci. Technol*. **38**, 775-782.

816   Zouari, N.; Mhiri, T.; Daoud, A.; Gravereau, P. and Lebraud, E. (2000). Crystal structure and

817   Rietveld refinement using X-ray powder diffraction data of two potassium and ammonium

818   - samarium condensed phosphates: K Sm H P3 O10 and N H4 Sm H P3 O10 *Int. J. Inorg.*

819   *Mater.* **2,** 379-387.

Figure Captions

822 **Figure 1**. Graphs showing (a) adsorption of Gd and suspension pH as a function of time, (b)

823 adsorption reversibility as exemplified by Er, (c) reproducibility of 3 suspensions of

824 ~0.2g/L biomass and 4 mg/L Er, and (d) comparison of fresh (FS) and freeze-dried (FZ)

825 cells of the same dry biomass concentration, showing that the use of freeze-dried does not

826 have an effect on the Nd adsorption edge. Note also that equilibration of pH and

827 adsorption occurs after 100 minutes or so.

828

829 **Figure 2**. Experimental adsorption data (symbols) and FITEQL model fits (curves) for the

830 adsorption of different lanthanides to *Pantoea agglomerans* cells. Model curves represent

831 adsorption to carboxyl (dotted line) and phosphate (solid line) sites respectively. Thus the

832 legend label "La2P" refers to a model curve predicted for the adsorption of 2mg/l

833 lanthanum assuming adsorption to a phosphate site whereas "La2C" refers to the same

834 model assuming adsorption to a carboxyl site etc.

835

836 **Figure 3**: k^3-weighted EXAFS, each shell's contribution to the EXAFS fit (shell 1 is above

837 shell 2 for each sample), and phase shifted Fourier transforms for (a) pH 6 4 mg/l Nd

838 sample, (b) pH6 10 mg/l Sm, (c) pH6 4 mg/l Sm and (d) pH 3.5 4 mg/l Sm samples.

839 Spectra have been offset for clarity. Experimental data is solid line and fit is dotted line.

840

841 **Figure 4**. k^3-weighted EXAFS, each shell's contribution to the EXAFS fit (shell 1 is above

842 shell 2 for each sample), and phase shifted Fourier transforms for (a) pH3.5, 4 mg/l Yb,

843 (b) pH3.5, 10 mg/l Yb (c) pH6 4 mg/l Yb and (d) pH6, 10 mg/l Yb samples, as well as (e)

844 pH3.5 4 mg/l Er and (f) pH 6 4 mg/l Er. Spectra have been offset for clarity. Experimental

845 514 data is solid line and fit is dotted line.

846

847
848   **Figure 5**. Molecular structures of N-acetylglucosamine-6-phosphate (redrawn from Nishitani

849   et al., 2006) and phosphatidylethanolamine (redrawn from Mayes, 1985), showing

850   possible phosphate groups that may be involved in lanthanide coordination on a gram-

851   negative bacterial cell surface. In practice, the cell surface composition is likely more

852   complex but the deprotonation constants for the different protons attached to the

853   phosphate group appear to have a relatively narrow range.

854
855 **Table Captions.**
856
857 **Table 1**. Compilation of experiments reported in this study, summarising the initial biomass

858 and lanthanide concentrations. Column 6 represents the *relative* metal to biomass ratio

859 between the 4 mg/L and the 2 mg/L suspensions, calculated by dividing the lanthanide to

860 biomass ratio for the 4 mg/L experiment by the corresponding ratio in the 2 mg/L

861 experiment.

862

863 **Table 2**. Results from FITEQL optimisation of stability constants for the adsorption of the

864 studied lanthanides, with errors on the mean representing one times the standard deviation.

865 Models were realised using bacterial deprotonation constants and surface site densities

866 determined by Ngwenya et al (2003). For carboxyl sites, the values are pKa = 4.3±0.2 and

867 site density = 5.0±0.7 mol/g cells, whereas the corresponding values for phosphate sites

868 are pKa= 6.9±0.5 and site density = 2.2±0.6 mol/g cells. The abbreviations "La2"

869 represent an experiment using 2 mg/L lanthanum, etc whereas ErUP and ErDN refer to

870 reversibility experiments in which the pH of the initial suspension was adjusted upwards

871 or downwards respectively.

872

873 **Table 3**. EXAFS analysis results for the lanthanide L3 edge collected in Fluorescence mode.

Table 1.

Element	Experiment	Biomass (g/L)	Log Molarity Initial $[Ln^{3+}]$	Lanthanide/Biomass (mol/g) x 10^{-4}	La4/ La2 metal/biomass ratio
Lanthanum	La2	0.125	-4.83	1.18	
	La4	0.2	-4.53	1.48	1.25
Neodymium	Nd2	0.19	-4.84	0.80	
	Nd4	0.25	-4.57	0.92	1.15
Samarium	Sm2	0.255	-4.86	0.54	
	Sm4	0.18	-4.63	1.30	2.41
Erbium	Er4	0.18	-4.57	1.51	
	Er4UP	0.21	-4.64	1.09	
	ER4DN	0.21	-4.64	1.09	
Ytterbium	Yb2	0.25	-4.92	0.48	
	Yb4	0.16	-4.67	1.34	2.79

Table 2.

Element	Experiment	R-COO-Ln2+		R-PO4-Ln2+	
		Log K	WSOS/DF	Log K	WSOS/DF
Lanthanum	La2	4.86	0.39	8.14	0.24
	La4	4.87	5.56	8.12	2.04
Mean ±1sd		4.86 ± 0.01		8.13 ± 0.01	
Neodymium	Nd2	5.34	0.03	8.53	0.32
	Nd4	4.78	1.24	8.46	0.45
Mean ±1sd		5.06±0.40		8.50±0.05	
Samarium	Sm2	5.15	0.16	8.37	0.51
	Sm4	5.10	0.77	8.33	1.58
Mean ±1sd		5.13 ± 0.03		8.35 ± 0.03	
Gadolinium	Gd4	5.14	0.80	8.40	0.70
Erbium	Er4	5.44	2.08	8.67	3.80
	Er4UP	5.21	0.46	8.43	0.15
	Er4DN	5.22	0.40	8.45	0.60
Mean ±1sd		5.29 ± 0.13		8.52 ± 0.13	
Ytterbium	Yb2	5.49	0.10	8.66	0.13
	Yb4	5.17	0.52	8.34	0.69
Mean ±1sd		5.33 ± 0.23		8.50 ± 0.23	

Table 3.

Sample	CN [a]	Atom Type	Shell Radius[b] (Å)	Debye-Waller factor (Å) [-2]	R Factor
Nd pH6, 4 mg/L	10.5	O	2.48	0.024	27.3
	4	P	3.92	0.024	
Sm pH 3.5, 4 mg/L	8	O	2.43	0.013	32.7
	4	P	3.85	0.016	
Sm pH 6, 4 mg/L	8	O	2.46	0.013	31.8
	5	C	3.64	0.030	
Sm pH 6, 10 mg/L	10	O	2.45	0.025	34.6
	6	C	3.48	0.004	
Er pH 3.5, 4 mg/L	7.5	O	2.39	0.022	38.7
	3	P	3.81	0.035	
Er pH 6, 4 mg/L	9	O	2.38	0.018	16.2
	5	P	3.83	0.040	
Yb pH 3.5, 4 mg/L	10	O	2.27	0.030	31.8
	4	P	3.80	0.016	
Yb pH 3.5, 10 mg/L	9	O	2.26	0.028	26.5
	4.5	P	3.74	0.021	
Yb pH 6, 4 mg/L	10	O	2.30	0.028	27.4
	2	P	3.77	0.016	
Yb pH 6, 10 mg/L	8	O	2.27	0.014	33.5
	4	P	3.75	0.033	

(a): ±15%; (b) ± 0.5 %

889
890
891
892
893
894
895
896
897
898
899
900
901

Figures

Figure 1, Ngwenya et al

(a) Time Course Experiment

(b) Reversibility test

(c) Reproducibility test

(d) Fresh and Freeze-dried cells

Figure 2, Ngwenya et al.

(a) Lanthanum

(b) Neodymium
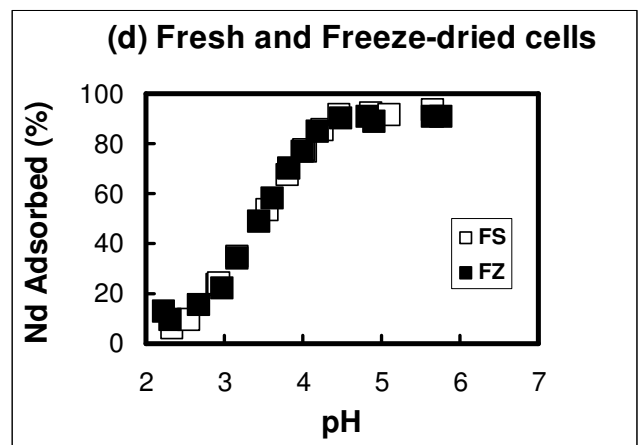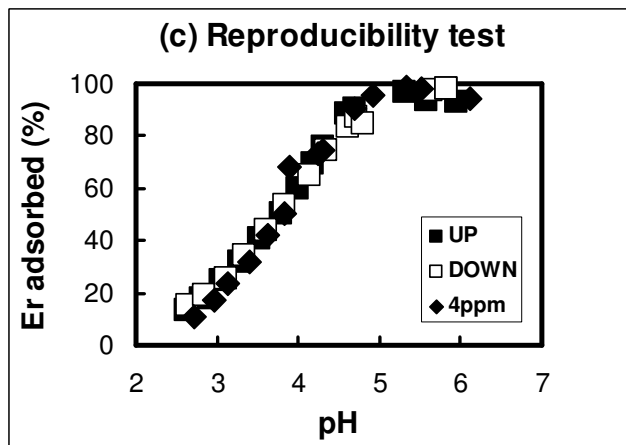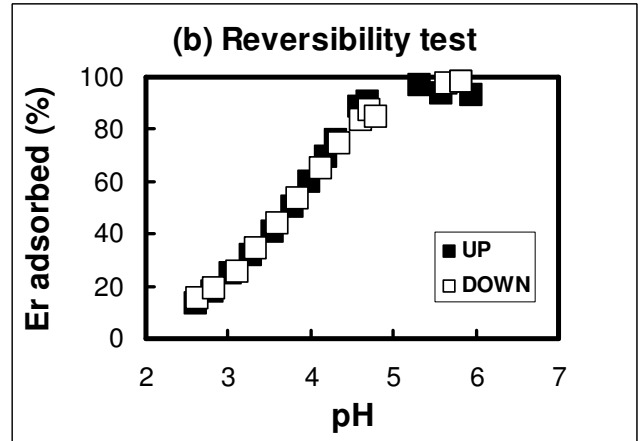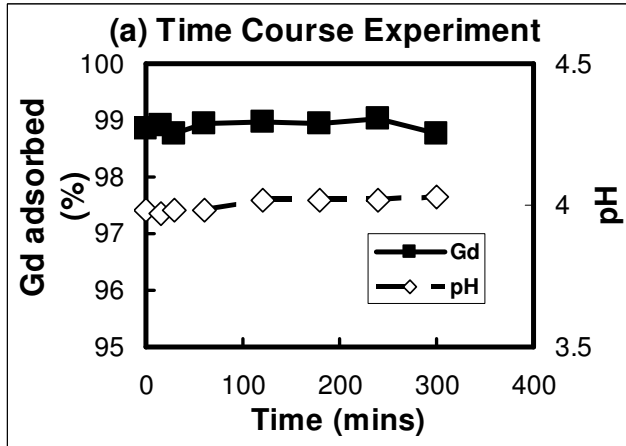
951
952
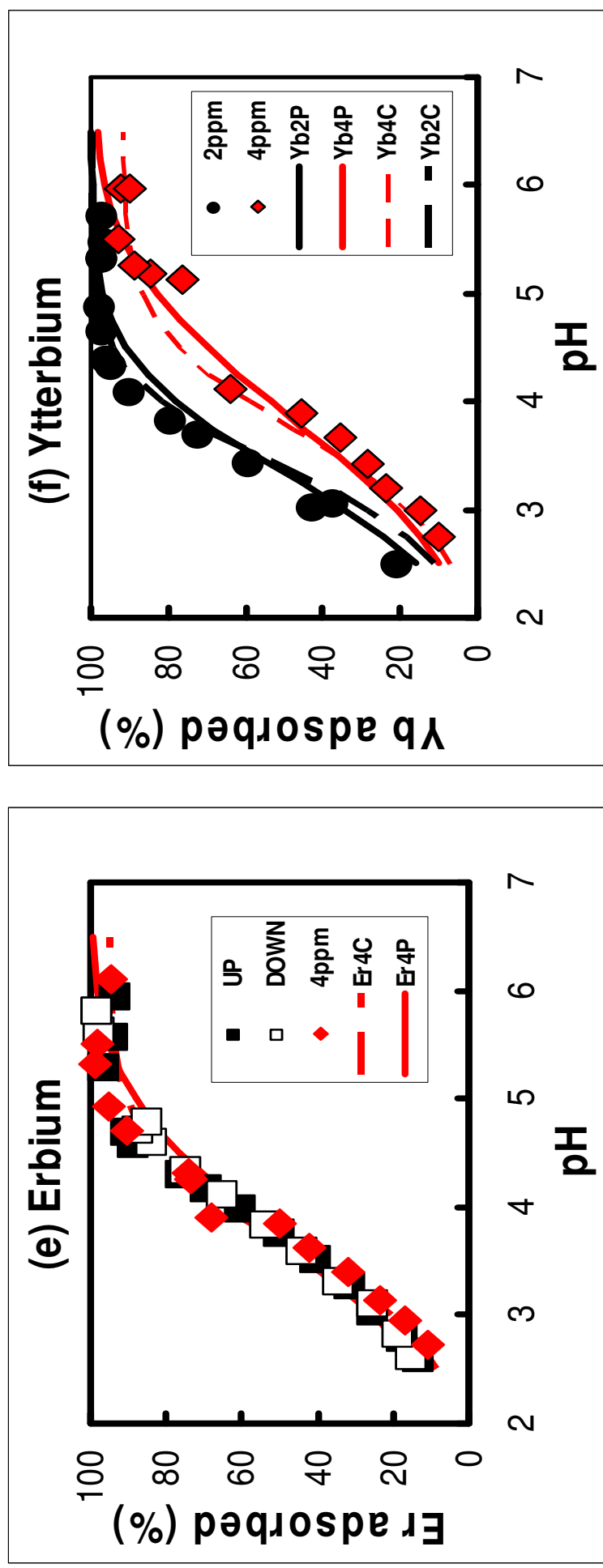953
954
955
956

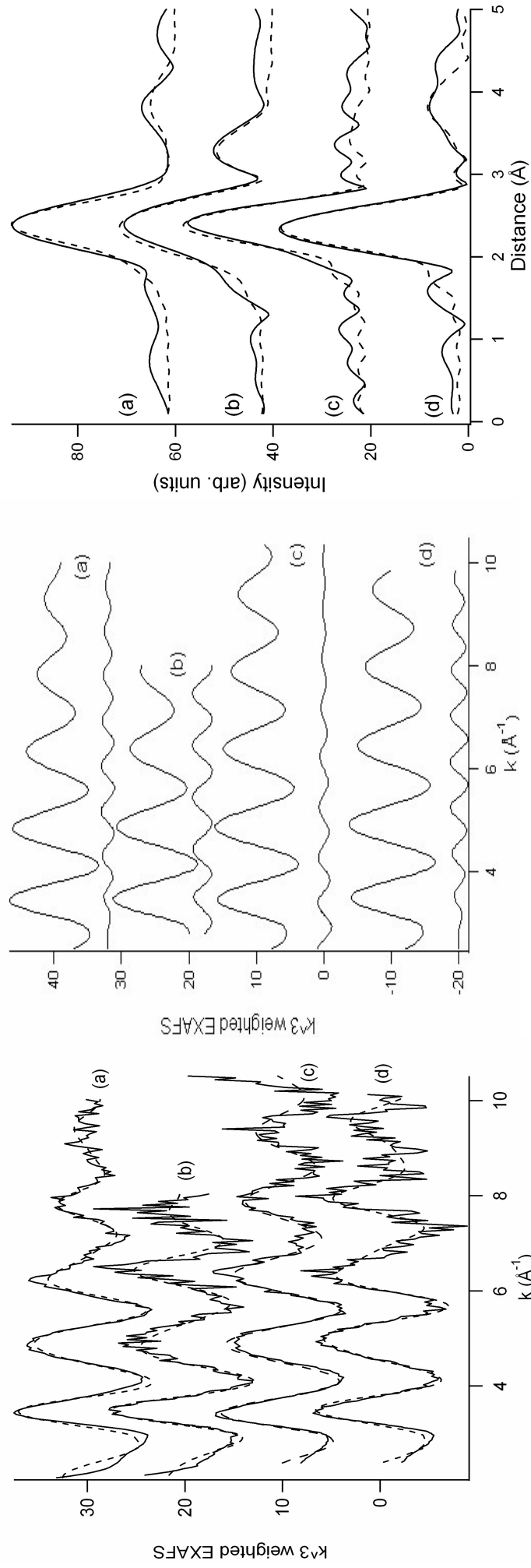**Figure 2 cont'd, Ngwenya et al.**

(c) Samarium

(d) Gadolinium
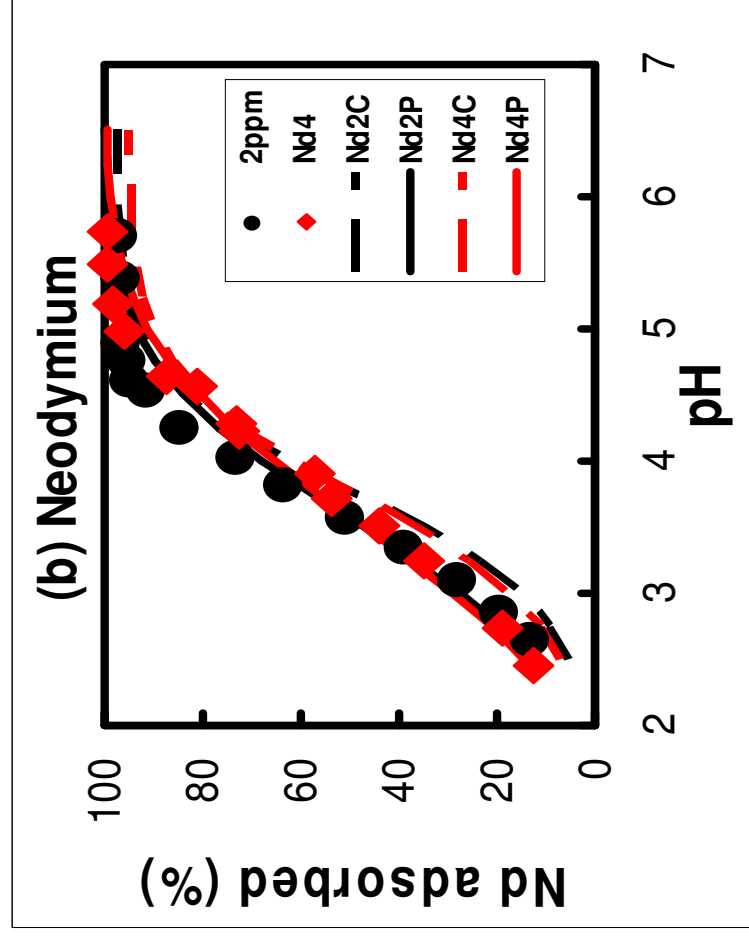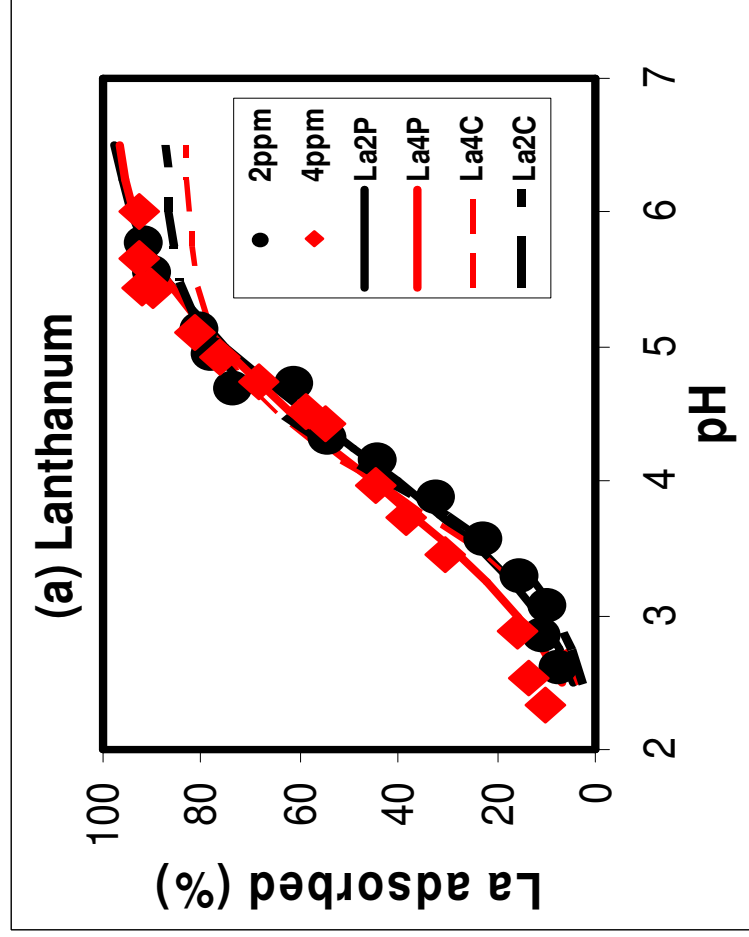
Figure 2 cont'd, Ngwenya et al.
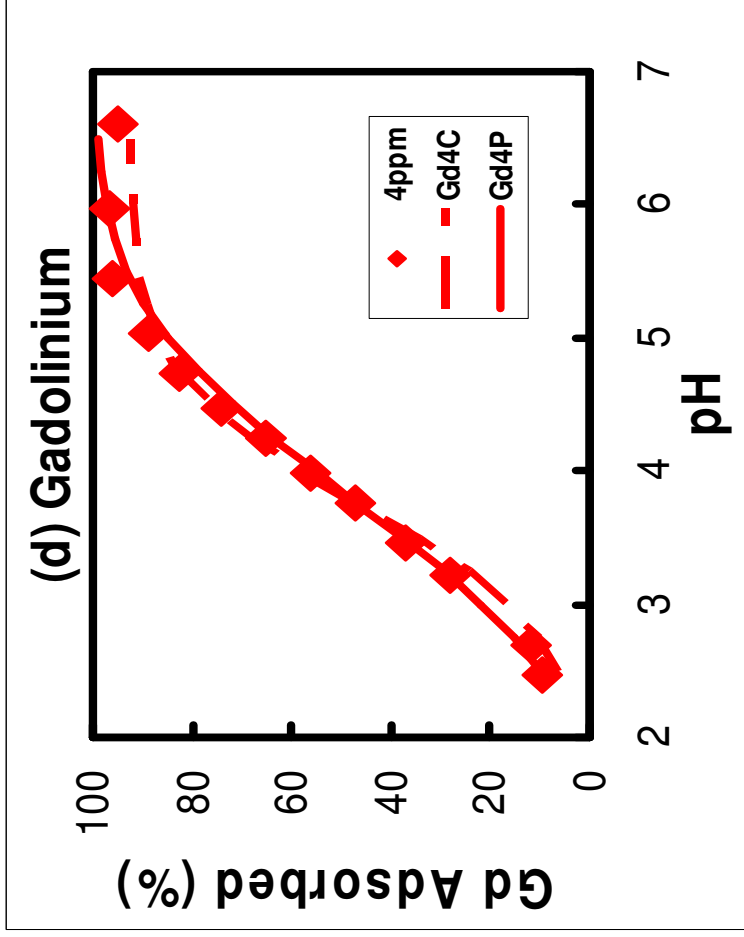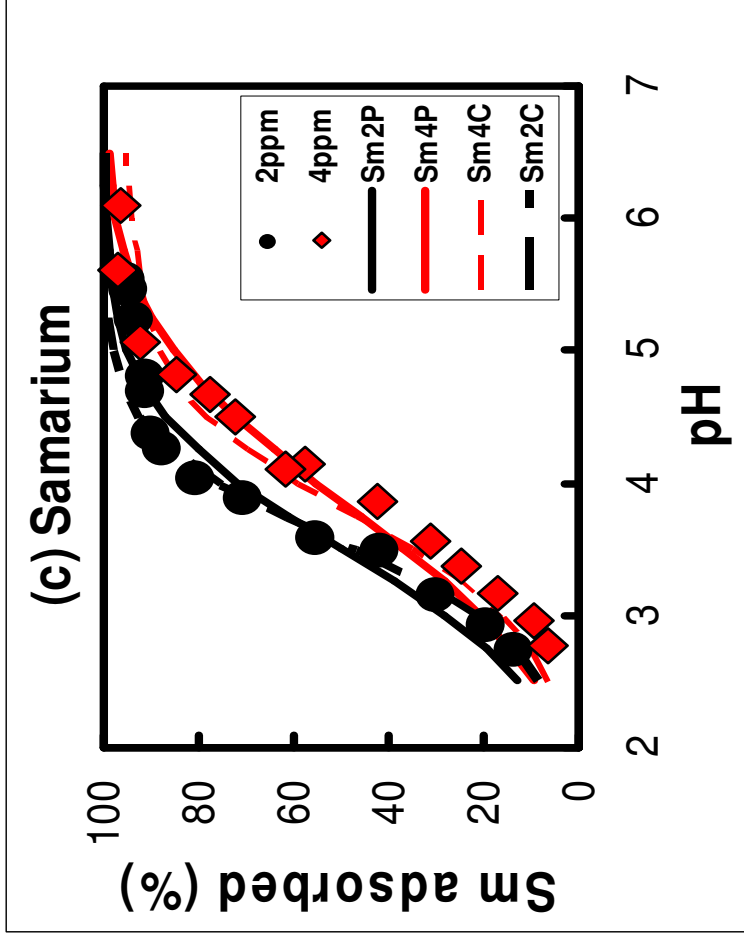
959
960
961
962
963
964
965
966

967
968
969
970
971
972
973
974
975
976
977
978
979
980
981
982
983
984
985
986
987
988
989
990
991
992
993
994
995
996
997
998
999
1000

Figure 3, Ngwenya et al.
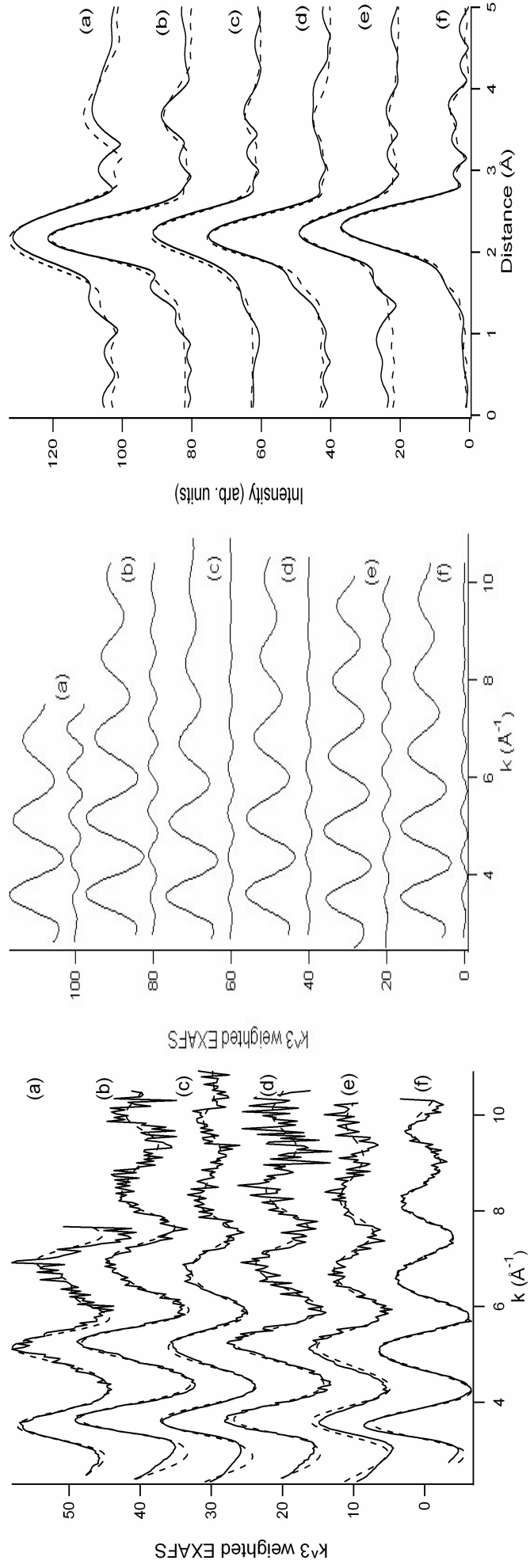
Figure 4, Ngwenya et al.

Figure 5, Ngwenya et al

(a) N-acetylglucosamine-6-phosphate

(b) Phosphatidylethanolamine